JOURNAL OF THERMOPHYSICS AND HEAT TRANSFER
Vol. 14, No. 3, July–September 2000

Heat Transfer Coefficient Measurement on Iced Airfoil in Small Icing Wind Tunnel

Robert C. Henry,* Didier Guffond,* François Garnier,* and André Bouveret†
ONERA, 92322 Châtillon Cedex, France

The local convective heat transfer coefficient distribution is measured on an iced airfoil in a small closed-loop icing tunnel at the Centre d'Essais des Propulseurs, the French engine test center. The airfoil surface is heated with a modulated laser source, and the heat flux variation of the ice is recorded with an infrared camera. The method is validated on a cylinder in dry air and in icing conditions. The method is then applied to a 145-mm-chord airfoil covered with typical rime, glaze, and mixed ice shapes. The effect of air velocity is studied by performing tests at airspeeds from 80 to 123 m/s (Reynolds numbers from 1.25×10^6 to 1.9×10^6). It was found that the heat transfer coefficient strongly depends on the surface condition of the ice. In relatively smooth zones, values are approximately equal to 400 W/m^2°C, whereas values greater than 1000 W/m^2°C are observed in nonuniform and rough areas. Results and limitations of the method are discussed and compared to numerical results obtained on similar ice shapes.

Nomenclature

b	= ice surface effusivity, W m^{-2} K^{-1} s$^{-1/2}$
C_p	= air specific heat
d	= cylinder diameter
Fr_d	= Frössling number based on cylinder diameter
f	= frequency of laser modulation
h	= global heat transfer coefficient
h_{conv}	= convective heat transfer coefficient
h_r	= radiative heat transfer coefficient
I_{conv}	= convective heat flux at surface of ice
I_{inc}	= incoming laser heat flux
I_r	= radiative heat loss flux at surface of ice
I_v	= evaporative heat flux at surface of ice
I_0	= maximum laser heat flux
k	= thermal conductivity of altuglass cylinder
L_{evap}	= evaporative latent heat flux
Nu_d	= Nusselt number based on cylinder diameter
P_s	= saturation vapor pressure
P_∞	= air freestream pressure
Re_d	= Reynolds number based on cylinder diameter
T_s	= ice surface temperature
T_w	= wind-tunnel wall temperature
T_∞	= freestream temperature
α	= incidence of the profile
ε	= emissivity
$\theta(x, t)$	= enhancement of ice surface temperature due to laser modulation
θ_0	= amplitude of temperature modulation
σ	= Stefan constant
φ	= phase lag
Ψ	= angle position of the cylinder
ω	= pulsation of laser modulation

Introduction

ICE accretion on a surface wing of aircraft poses a serious threat to flight safety. In particular, glaze ice deposit can affect dramatically the flight performance. If ice accretion effects are to be minimized, a prediction method for its formation is required. Therefore, two-dimensional and three-dimensional models have been developed to predict and reproduce ice accretion shapes on profiles. However, severe glaze ice shape cannot be predicted with a good accuracy due to limitations of heat transfer models taking into account the ice roughness.

The convective heat transfer distribution on iced surfaces has been identified as a determinant parameter for ice accretion simulation. Heat transfer analysis used in current models is based on equivalent sand-grain correlations developed by Nikuradse[1] and Schlichting,[2] which cannot be always representative of complex geometry and surface roughness of ice shape.

Consequently, various experimental methods have been used to measure the local heat transfer coefficient and to determine the influence of surface roughness. Most of these methods are based on measurements on casted iced airfoil models covered with artificial roughness. Achenbach[3] and Arimilli et al.[4] used cylinders with simulated wooden ice shapes and Poinsatte et al.[5] arranged heat flux gauges on an airfoil covered with hemispherical roughness elements.

Recently, an improvement of the frozen ice shape casting technique allowed Dukhane et al.[6] to measure the heat transfer of more representative ice surface models in a dry wind tunnel. However, the heat transfer measurements have always been performed on the ice model rather than on the ice shape itself.

At the same time, an infrared technique, used by Hansman and Yamaguchi[7] to investigate laminar/turbulent transition on an iced surface was adapted to the heat transfer characterization of roughness elements by Henry[8] and was applied to measurements on an airfoil with simulated ice roughness by Bragg et al.[9]

This paper presents a further application of the infrared technique to map out the heat transfer coefficient on a real ice shape, formed on an airfoil in an icing wind tunnel.

Experimental Method

The experimental approach involves measurement of the local heat transfer coefficient on an ice accretion during a dry air sequence following icing conditions. The ice surface is heated with a modulated laser source, and temperature enhancement is monitored with an infrared camera. The heat transfer coefficient is then calculated from the temperature oscillation. An advantage of this method is that the result is independent of the initial temperature and outside conditions.

Thermal Analysis

During these measurements, the iced airfoil is kept in the cold airflow and is heated by the laser modulated heat flux:

$$I_{\text{inc}}(\omega, t) = I_0 a + I_0 m \sin \omega t \tag{1}$$

Received 29 March 1999; revision received 19 October 1999; accepted for publication 22 October 1999.

*Research Scientist, Physics, Instrumentation, and Sensing Department.
†Research Scientist, Solid and Dammage Mechanics Department.

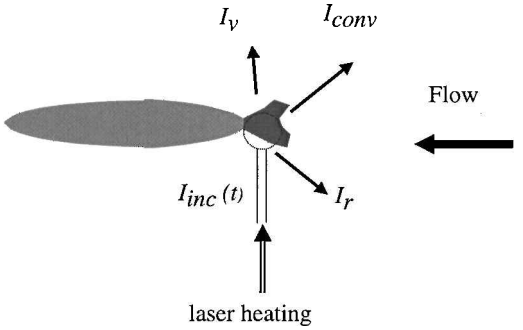

Fig. 1 Ice surface heat flux balance during heat transfer coefficient measurement.

where I_0a and I_0m are the mean and the modulated components of the laser heat flux, respectively. The heat flux losses at the ice surface can be defined by the three following terms (Fig. 1).

The convective heat flux I_{conv} is given by

$$I_{conv} = h_{conv}(T_S - T_\infty) \tag{2}$$

The evaporative heat flux I_v is related to convective heat transfer coefficient by the relationship[10]

$$I_v = 0.694 h_{conv} L_{evap}[P_S(T_S) - P_S(T_\infty)]/C_p P_\infty \tag{3}$$

The radiative loss I_r is given by

$$I_r = \varepsilon\sigma\left(T_s^4 - T_w^4\right) \tag{4}$$

At the ice surface, $\theta(x, t)$, the temperature enhancement induced by the laser modulation can be described by the one-dimensional energy equation

$$\kappa\frac{\partial^2\theta}{\partial x^2} = \frac{\partial\theta}{\partial t} \tag{5}$$

Boundary conditions at the ice surface are given by

$$k\left(\frac{\partial\theta}{\partial x}\right) = I_{conv}(\theta) + I_v(\theta) + I_r(\theta) - mI_0\sin\omega t \tag{6}$$

$$\theta(x = \infty, t) = 0 \tag{7}$$

$$\theta(x, 0) = 0 \tag{8}$$

Equation (6) gives the heat flux at the ice surface and can be written as

$$k\left(\frac{\partial\theta}{\partial x}\right) = h\,\theta(0, t) - mI_0\sin\omega t \tag{9}$$

where h is the global heat transfer coefficient, including convective, evaporative, and radiative losses:

$$h = (1 + q_v)h_{conv} + h_r \tag{10}$$

where $q_v = \alpha + \beta\theta(0, t)$ is a correction term for the evaporative flux and α and β are coefficients depending on the total temperature. For example, $\alpha = 0.557$ and $\beta = 0.06$ for a total temperature of 263 K. Furthermore, the radiative heat transfer coefficient h_r can be expressed by the following expression: $h_r \approx 4\varepsilon\sigma T_s^3$. This term is small in comparison to h_{conv} and can, therefore, be neglected ($h_r/h_{conv} \approx 0.5\%$).

Heat Transfer Coefficient Calculation

A solution of Eq. (5) is given by the fundamental sinusoidal temperature oscillation[11]

$$\theta(x, t) = \theta_0\exp(-\sqrt{\omega/2\kappa}x)\sin(\omega t + \varphi) \tag{11}$$

Theoretically, the value of h can be extracted from either the amplitude or the phase. Calculation from the phase simply requires the value of ω, whereas calculation from the amplitude further necessitates the value of the power density mI_0. Thus, in present analysis, h is calculated from the phase and can be written by introducing the ice effusivity b and the frequency of the modulated laser source, f,

$$h = -b\sqrt{\pi f}[1/\tan\varphi(x = 0) + 1] \tag{12}$$

and, finally, h can be expressed as a function of measured phase lag,

$$h = b\sqrt{\pi f}\frac{2\tan\left(\varphi^{mes} - \varphi_0^{mes}\right)}{1 - \tan\left(\varphi^{mes} - \varphi_0^{mes}\right)} \tag{13}$$

where φ^{mes} is the phase lag measured by the infrared camera on each pixel of the ice surface during tunnel test runs with airflow and φ_0^{mes} is a reference phase lag due to components measured without airflow.

The infrared picture of the phase lag is deduced from a synchronous detection method commonly used in nondestructive evaluation of materials.[12] This method is based on the storage of infrared frames whose starting times coincide with a particular phase of the modulated heat signals.

Limitation and Accuracy of Method

Theoretically, the accuracy of the heat transfer coefficient measurement depends directly on the accuracy of the phase detemination φ^{mes}. A sensibility value of 10^{-4} on the phase value conducts to a good prediction of the heat transfer accuracy ($\Delta h/h \cong 1\%$). However, the following hypotheses have to be applied for the calculation of h, which can reduce the final accuracy on the method on the order of 15%: 1) Heat transfer is supposed normal to the surface (one dimensional). 2) Ice is considered a semi-infinite wall. 3) Heat radiation is supposed absorbed by the surface, that is, a 3-mm minimum ice thickness is required.

Experimental Procedure

Model and Wind Tunnel

Heat transfer measurements are performed in a closed-loop icing wind tunnel at the Centre d'Essais des Propulseurs (CEPr) (Propulsion Test Center). The design of PAG is shown in Fig. 2.

Measurements are conducted on a 30-mm-diam cylinder and a 145-mm-chord airfoil, 17 mm in thickness. Both are mounted vertically in the 20 × 20 cm test section. A 100-mm-diam ZnSe window, transparent to infrared radiation, is centered on one of the glass sidewalls of the wind tunnel.

Laser and Optical Apparatus

The 10.6-μm wavelength CO_2 laser beam is especially appropriate for the present test because ice properties are very close to those of a blackbody at this wavelength. The nominal laser power is 17 W, and the laser beam is homogenized in a cavity. The power density is approximately 0.15 W cm^{-2} in a 5 × 5 cm field. Modulation of the laser signal is obtained by two rotating disk blades, spinning at a 0.1-Hz frequency.

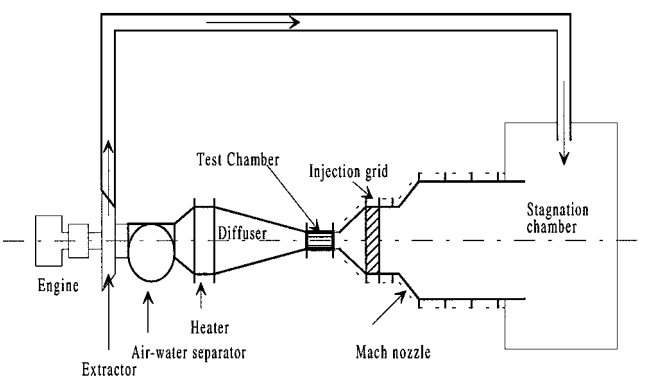

Fig. 2 Scheme of the icing test facility.

Infrared Camera

A 3–5-μm infrared (IR) camera is used. The relative low response of the camera at low temperatures is compensated for by its high sensitivity, due to its 128 × 128 sensor matrix. The typical noise level is 0.007 K on a pixel.

Because the IR camera view and laser beam paths are seen through the same ZnSe window (Fig. 3), the camera is placed close to the laser and perpendicular to the flow direction, viewing the test model from the side.

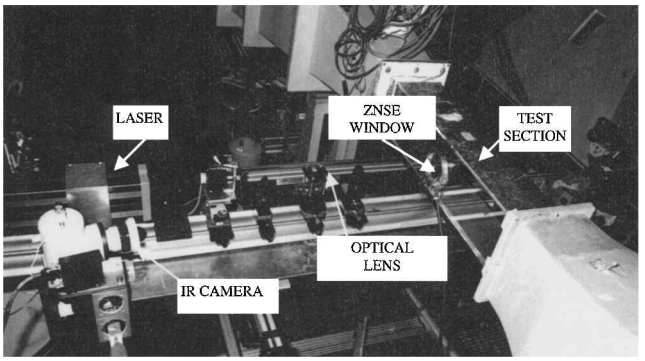

Fig. 3 General view of test setup.

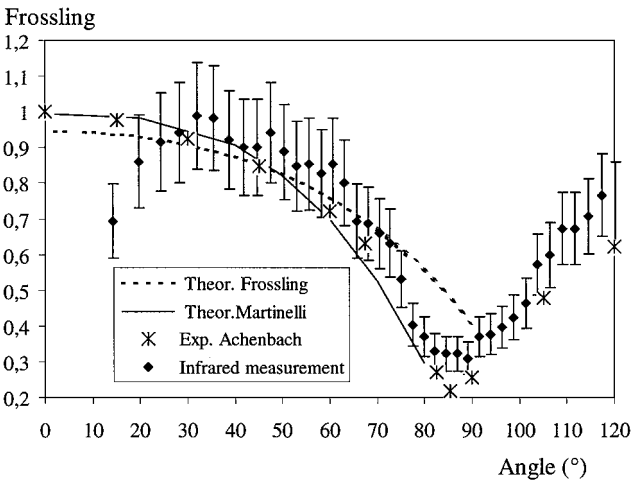

Fig. 4 Frossling numbers on a cylinder ($Re = 1.41 \times 10^5$); comparison between IR measurements, theoretical values, and Achenbach data.[15]

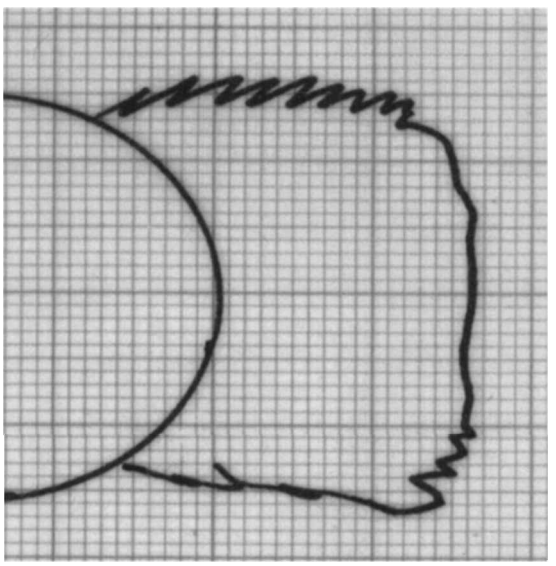

Fig. 5a Flat rime ice accretion tracing on a cylinder: $V = 70$ m/s, $T_\infty = -25°C$, and $t = 270$ s.

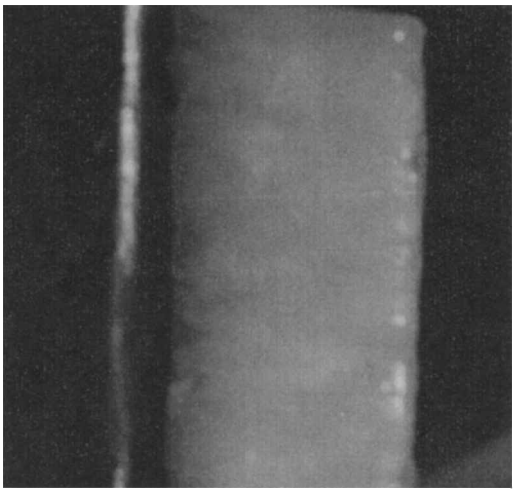

Fig. 5b Rime ice on a cylinder (lower side view): $V = 70$ m/s, $T_\infty = -25°C$, and $t = 270$ s.

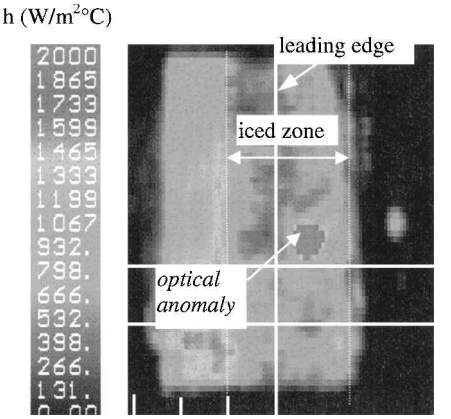

Fig. 5c Heat transfer coefficient IR map: $V = 70$ m/s, $T_\infty = -25°C$, and $t = 270$ s.

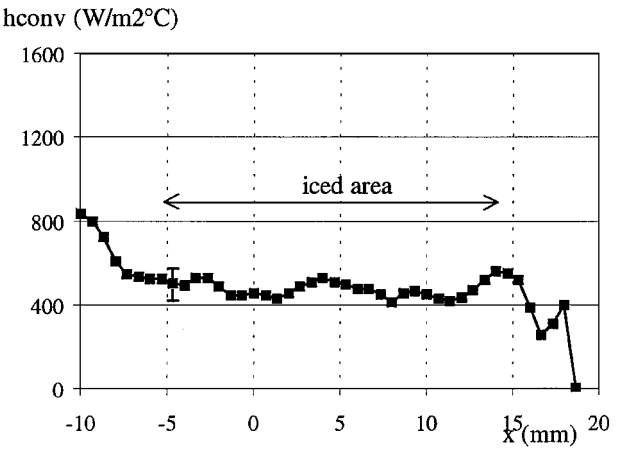

Fig. 5d Convective heat transfer profile on a cylinder; rime ice case: $V = 70$ m/s, $T_\infty = -25°C$, and $t = 270$ s.

Test Procedure

After the ice shape forms on the test model, the water spray is stopped while the airspeed is kept constant and the temperature is kept cold. The modulated laser source is powered, and the IR signal is recorded for approximately 30 s, increasing the ice surface temperature amplitude less than 2°C to avoid melting the ice. The airflow is then stopped, and a sequence is recorded to determine the reference phase signal. Phase maps are generated and heat transfer coefficient values are calculated from Eq. (13).

Experimental Results and Discussion

Validation on Smooth Cylinder

The test method is first validated on an altuglass cylinder in dry air at an airspeed of 70 m/s. Values of the local heat transfer coefficient obtained with this method are compared with theroretical values from Frossling,[13] empirical values,[14] and experimental data obtained by Achenbach.[15] Heat transfer coefficient values are reduced to the Frössling number based on the 30-mm-cylinder diameter:

$$Fr_d = Nu_d / \sqrt{Re_d} \tag{14}$$

The Nusselt number is related to the local heat transfer coefficient h through the relationship

$$Nu_d = hd/k \tag{15}$$

The Reynolds number, related to the cylinder diameter, is 1.41×10^5. Frossling number is plotted vs the angle position of the cylinder in Fig. 4. Values decrease with increasing angle until flow separation occurs and increases thereafter (90-deg value is normal to the flowfield). IR measurements are inside a 15% error bar. A larger discrepancy between the present experiment and the other data is noticed close to the leading edge (angle 0–30 deg). This is because the incoming heat flux is lower at the leading edge because the laser flux is perpendicular to the test model and because the one-dimensional heat transfer model is not very appropriate in this area.

Measurements on Iced Cylinder

In the present study, rime ice shapes are obtained on the cylinder at a static temperature of −25°C, a velocity of 70 m/s, a liquid water content (LWC) of 1 g/m^3, and a mean volume diameter (MVD) of 20 μm.

A tracing of the ice shape at $t = 270$ s is shown in Fig. 5a. The ice deposit is 15 mm thick, and the front surface is flat. A lateral view of the ice shape (Fig. 5b) shows a relatively smooth surface.

An IR picture taken from the same view is shown in Fig. 5c. The stagnation line of the cylinder and ice limit extensions are highlighted. The image is calibrated by the global heat transfer coefficient before applying the evaporative correction. Note that the values are not uniform, especially in the vertical direction. The spot located at the center of picture is an optical anomaly due to a reflection.

The convective heat transfer distribution is plotted vs the abscissa in Fig. 5d. This profile is obtained from an IR picture by averaging values in the vertical zone delimited by the horizontal lines represented in Fig. 5c. The abscissa $x = 0$ is referenced as the cylinder stagnation point, and ice extends approximately from $x = -5$ to +15 mm. Values of the convective heat transfer coefficient extend from 400 to 600 W/m^2°C after the evaporative correction is applied.

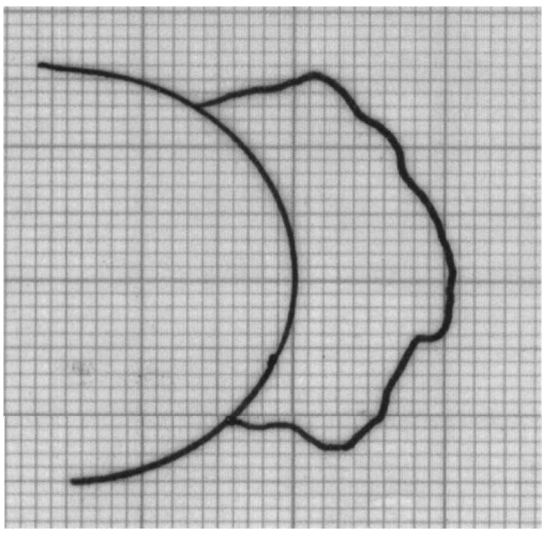

Fig. 6a Mixed ice accretion tracing on a cylinder: $V = 75$ m/s, $T_\infty = -25$°C, and $t = 240$ s.

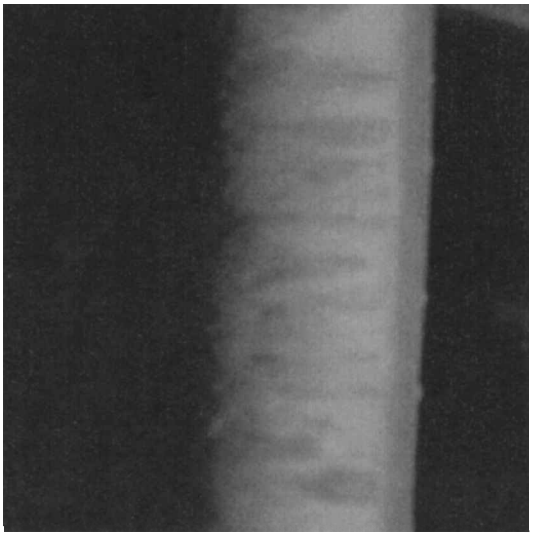

Fig. 6b Mixed ice on a cylinder (lower side view): $V = 75$ m/s, $T_\infty = -25$°C, and $t = 240$ s.

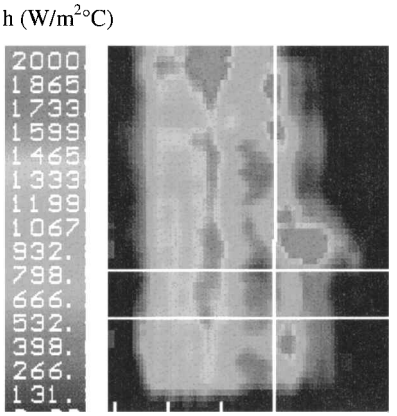

Fig. 6c Heat transfer coefficient IR map: $V = 75$ m/s, $T_\infty = -25$°C, and $t = 240$ s.

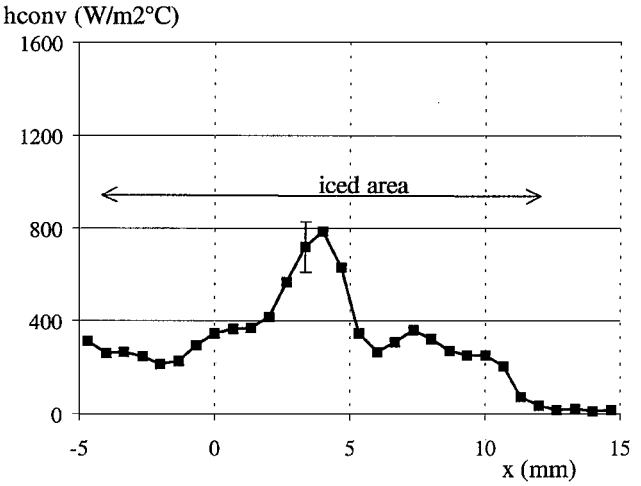

Fig. 6d Convective heat transfer profile on a cylinder; mixed ice case: $V = 75$ m/s, $T_\infty = -25$°C, and $t = 240$ s.

At the same temperature, an airspeed of 75 m/s, and a shorter ice accretion time (240 s), a mixed ice shape with beginning horn formation is obtained (Figs. 6a and 6b). The heat transfer coefficient is shown in Fig. 6c, and the convective coefficient profile is plotted in Fig. 6d. Compared to the rime ice case, a peak value of 800 W/m^2°C is seen at the location of the development of the horns.

Measurements on Iced Airfoil

Similar measurements are made on a 145-mm-chord airfoil at 4-deg angle of attack, for rime and glaze ice accretions. The rime ice accretion is formed at a static temperature of −23°C, an airspeed of 80 m/s, LWC = 1 g/m^3, MVD = 20 μm, and an accretion time of 180 s.

An ice shape tracing is plotted in Fig. 7a. A closeup view of the lower side of the airfoil (Fig. 7b) shows three different ice zones: upstream, a uniform smooth zone 10 mm wide; then a rough zone 15 mm wide; and finally a region covered with scattered ice feathers.

These different zones can be identified on the heat transfer IR picture of the lower side of the airfoil (Fig. 7c). In the smooth zone, the heat transfer coefficient is uniform in both directions and has a value approximately 400 W/m^2°C. The values increase and become less uniform due to increasing roughness. Downstream, in the feathers region, values increase to a value of 2000 W/m^2°C. Note that measurement is less accurate in this region because the ice thickness can be smaller than the minimum value required by the IR method.

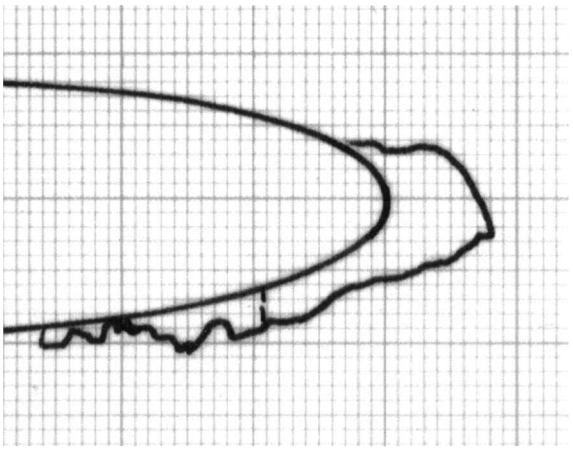

Fig. 7a Rime ice shape tracing on an airfoil: V = 80 m/s, T_∞ = − 23°C, t = 180 s, and α = 4 deg.

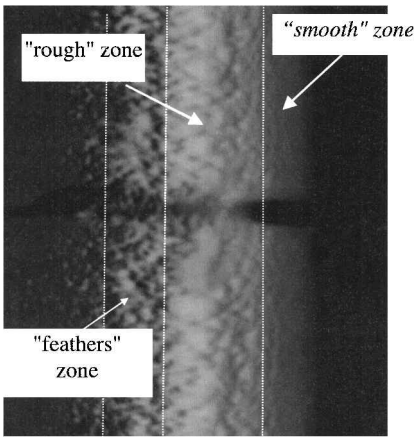

Fig. 7b Rime ice picture on an airfoil (lower side view): V = 80 m/s, T_∞ = − 23°C, t = 180 s, and α = 4 deg.

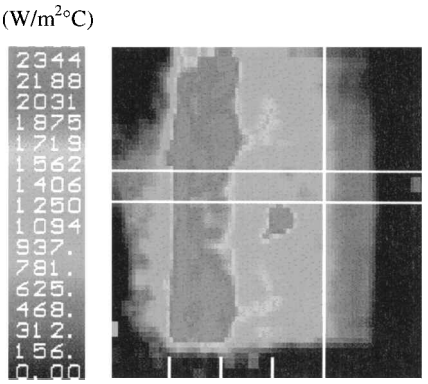

Fig. 7c Heat transfer coefficient IR map: V = 123 m/s, T_∞ = − 23°C, t = 180 s, and α = 4 deg.

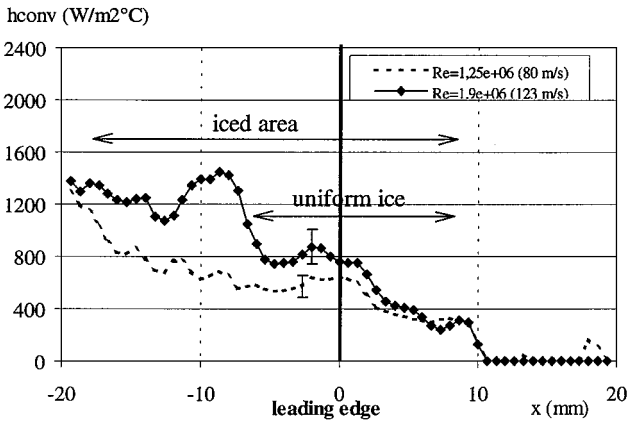

Fig. 7d Convective heat transfer profile on an airfoil; rime ice case: V = 80 and 123 m/s, T_∞ = − 23°C, t = 180 s, and α = 4 deg.

Influence of airspeed on the heat transfer coefficient is investigated by conducting a second measurement at 123 m/s. Convective heat transfer coefficient profiles are plotted vs the abscissa of the lower side in Fig. 7d for both airspeed values. In the smooth zone located upstream of the airfoil leading edge, the convective coefficient value is 400 W/m^2°C for both airspeed conditions, which can be related to laminar air flow conditions. In the rough zone, the values increase to reach 800 W/m^2°C for the lower airspeed and 1200 W/m^2°C for the higher airspeed. This can be explained by the development of airflow transition in the rough zone.

The heat transfer coefficient is measured on a glaze ice shape shown in Figs. 8a and 8b. This ice shape with double horns is obtained at a temperature of −19°C, at an airspeed of 130 m/s, LWC = 1 g/m^3, MVD = 20 μm, and at an accretion time of 180 s. The horns are 25 mm thick, and the surface is clear and smooth. Downstream, small feathers cover the airfoil up to the accretion limit.

The upper horn is seen at the right edge of the IR picture (Fig. 8c). Heat transfer is enhanced at this location. Downstream, a dark band corresponds to the stagnation region, which is not lighted by the heat source due to the shadow of the lower horn. Then, heat transfer values increase sharply on the second horn and decrease downstream. Maximum values are 1000 W/m^2°C at the horn location and decrease to 400 W/m^2°C downstream (Fig. 8d). Speculation is that a flowfield separation occurs behind the horns.

Comparison with Numerical Results

These experimental results are compared with calculations computed with the ONERA two-dimensional ice accretion code.[7] Based on a potential flow, the heat transfer coefficient is calculated by using an integral boundary-layer approach including Makonnen correlation[16] for the ice roughness effect. The Reynolds number relative to a normalized (divided by the chord) equivalent sand-grain roughness height equal to 0.001 is computed. For local Reynolds number less than 600, the local heat transfer coefficient is supposed laminar and is not dependent on the local roughness. For Reynolds greater than 600, the heat transfer coefficient is directly dependent on the roughness and is calculated using a turbulent flow approach.[17]

For the rime ice case on the airfoil described earlier (Figs. 7a–7d), comparison shows good agreement downstream of the leading edge (Fig. 9). At the stagnation point, located approximately at x = 4 mm, a jump can be noticed on the numerical curve due to a laminar/turbulent transition that is not observed on the experimental curve. At the ice tip (x = 7 mm), the calculated values increase sharply, unlike the experimental results. These results are thought to be overestimated due to a sharp geometry, conducting to a flowfield

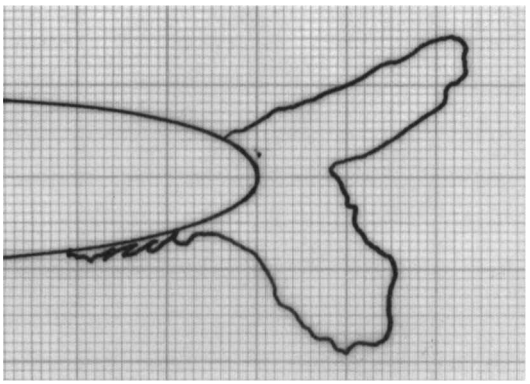

Fig. 8a Glaze ice shape tracing on an airfoil: $V = 130$ m/s, $T_\infty = -19°C$, $t = 180$ s, and $\alpha = 4$ deg.

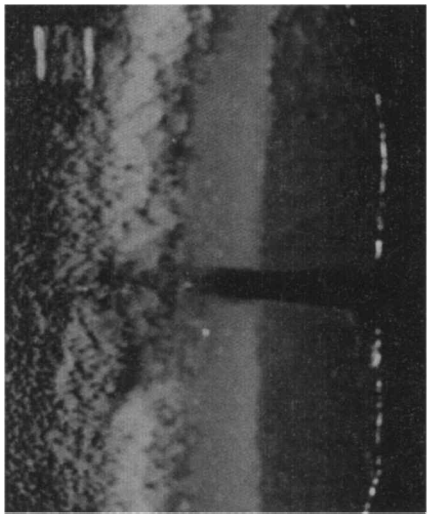

Fig. 8b Glaze ice on an airfoil (lower side view), $V = 130$ m/s, $T_\infty = -19°C$, $t = 180$ s, and $\alpha = 4$ deg.

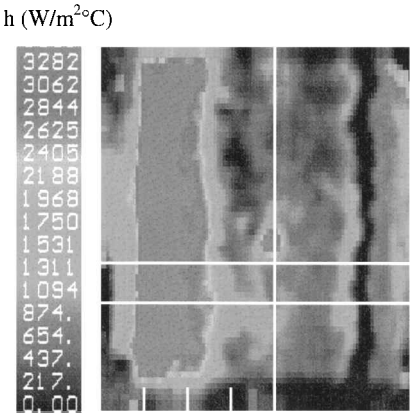

Fig. 8c Heat transfer coefficient IR map: $V = 130$ m/s, $T_\infty = -19°C$, $t = 180$ s, and $\alpha = 4$ deg.

separation. However, the reliability of the experiment is also lower in this region because of the grazing angle of view and the one-dimensional heat transfer hypothesis for the convective coefficient determination.

The heat transfer profile of glaze ice shape plotted in Fig. 10 shows differences between the curves. Discrepancies can be explained by limitations of the potential flow method. In the horn region, a separation/reattachment occurs and is not taken into account by the model. Consequently, calculated flow velocity and heat transfer coefficient at the horn location may be larger than the actual values.[18] Present measurements confirm this behavior.

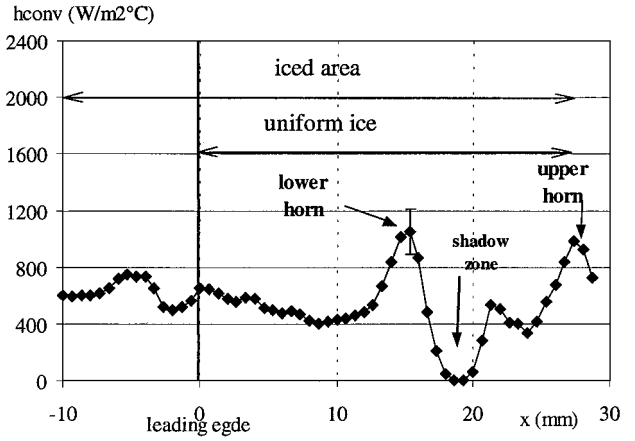

Fig. 8d Convective heat transfer profile on an airfoil; glaze ice case: $V = 130$ m/s, $T_\infty = -19°C$, $t = 180$ s, and $\alpha = 4$ deg.

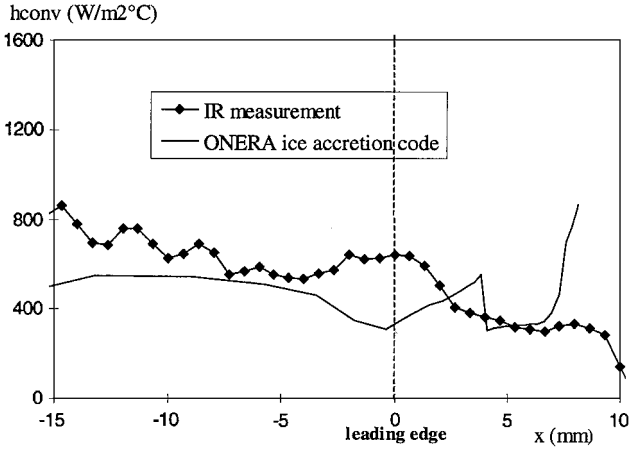

Fig. 9 Comparison between measured and calculated heat transfer coefficient profile on a rime ice accretion on an airfoil: $V = 80$ m/s, $T_\infty = -23°C$, $t = 180$ s, and $\alpha = 4$ deg.

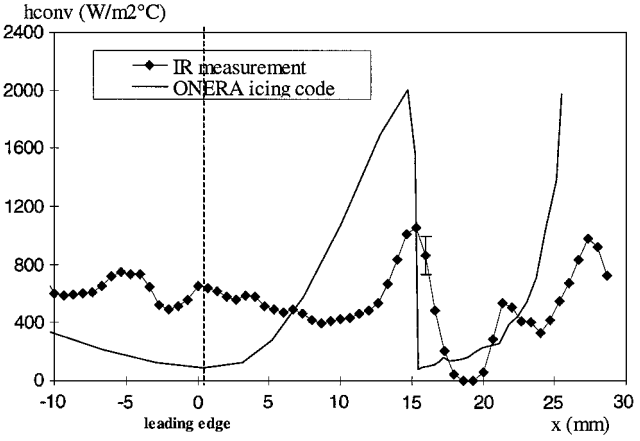

Fig. 10 Comparison between measured heat transfer coefficient and calculated profile on glaze ice accretion on an airfoil: $V = 130$ m/s, $T_\infty = -19°C$, $t = 180$ s, and $\alpha = 4$ deg.

Conclusion

The local heat transfer distribution was successfully measured on a real ice shape in a small wind tunnel. The method used a modulated laser source for heating the lower side of a test model. A heat transfer coefficient map was calculated from a temperature oscillation signal. The method is first validated on a cylinder in dry air and then applied to ice shapes formed on the cylinder.

1) On rime ice shapes, heat transfer values are found to be constant and approximately equal to 400 W/m^2°C.

2) On mixed ice shapes, enhancement is observed at the edge of the ice shape where horns start growing.

3) This behavior is confirmed on the iced airfoil. Convective heat transfer coefficient values are low and constant on smooth and uniform iced surface areas and increase in regions covered with roughness and ice feathers. Peak values are also observed at the horn tips of glaze ice shapes.

4) Comparison with results computed by the ONERA icing code based on a potential flow shows relatively good agreement on smooth surfaces and confirms overestimation of the calculation of heat transfer coefficient in the horn region. Enhancement of the heat transfer in regions covered with ice feathers is not well predicted.

5) More accurate results can be obtained in the future by applying this method to a full-scale test model in a large wind tunnel, allowing a better optical resolution at the leading edge.

Acknowledgments

This work was supported by Le Service des Programmes Aéronautiques. The authors wish to extend their appreciation to the Centre d'Essais des Propulseurs for use of their icing facilities.

References

[1]Nikuradse, J., "Laws of Flow in Rough Pipes," NACA TM-1292, 1933.

[2]Schlichting, H., *Boundary Layer Theory*, 6th ed, McGraw–Hill, New York, 1968, pp. 579–589.

[3]Achenbach, E., "The Effect of Surface Roughness on the Heat Transfer from a Circular Cylinder," *International Journal of Heat and Mass Transfer*, Vol. 20, 1977, pp. 359–369.

[4]Arimilli, R. V., Keshock, E. G., Poinsatte, P. E., and Van Fossen, G. J., "Measurements of Local Convective Heat Transfer Coefficients on Ice Accretion Shapes," AIAA Paper 84-0018, Jan. 1984.

[5]Poinsatte, P. E., Van Fossen, G. J., and De Witt, K. J., "Convective Heat Transfer Measurements from a NACA 0012 Airfoil in Flight and in the NASA Lewis Icing Research Tunnel," AIAA Paper 90-0199, Jan. 1990.

[6]Dukhan, N., Van Fossen, G. J., Masiulaniec, K., and Dewitt, K. J., "Convective Heat Transfer Coefficients from Various Types of Ice Roughened Surfaces in Parallel and Accelerating Flow," AIAA Paper 96-0867, Jan. 1996.

[7]Hansman, R. J., and Yamaguchi, K., "Modeling of Surface Roughness Effects on Glaze Ice Accretion," AIAA Paper 89-0734, Jan. 1989.

[8]Henry, R., Hansman, R. J., and Breuer, K., "Heat Transfer Variation on Protuberances and Surface Roughness Elements," *Journal of Thermophysics and Heat Transfer*, Vol. 9, No. 1, 1995, pp.175–180.

[9]Bragg, M. B., Cummings, S. L., and Henze, C. M., "Boundary-Layer and Heat-Transfer Measurements on an Airfoil with Simulated Ice Roughness," AIAA Paper 96-0866, Jan. 1996.

[10]Cansdale, J. T., and Gent, R. W., "Ice Accretion on Airfoils in Two-Dimensional Compressible Flow: A Theoretical Model," Royal Airforce Establishment, RAE-TR 82128, Farnborough, England, U.K., Jan. 1983.

[11]Carslaw, H. S., and Jaeger, J. C., *Conduction of Heat in Solids*, 2nd ed., Oxford Univ. Press, London, 1959, pp. 74–319.

[12]Krapez, J. C., Gardette, G., and Balageas, D., "Lock-In Infrared Thermography: Advantages and Problems of some Approaches," 3nd International Workshop on Advanced Infrared Technologies and Applications, Capri, Italy, 1995.

[13]Frossling, N., "Evaporation, Heat Transfer, and Velocity Distribution in Two-Dimensional and Rotationally Symmetrical Laminar Boundary-Layer Flow," NACA TM-1432, 1958.

[14]Boelter, L. M., Grossman, L. M., Martinelli, R. G., and Morin, E. H., "An Investigation of Aircraft Heaters. XXIX: Comparison of Several Methods of Calculating Heat Losses from Airfoils," NACA TN-1453, Oct. 1968, p. 75.

[15]Achenbach, E., "Total and Local Heat Transfer from a Smooth Circular Cylinder in a Cross-Flow at High Reynolds Number," *International Journal of Heat and Mass Transfer*, Vol. 18, 1975, pp. 1387–1396.

[16]Makkonen, L., "Heat Transfer and Icing of a Rough Cylinder," National Research Council of Canada, Rept. 23312, Ottawa, ON, Canada, 1984.

[17]Kays, W. M., and Crawford, M. E., *Convective Heat Mass Transfer*, 2nd ed, McGraw–Hill, New York, 1980, p. 420.

[18]Wright, W. B., Gent, R. W., and Guffond D., "DRA/NASA/ONERA Collaboration on Icing Research: Part II-Prediction of Airfoil Ice Accretion," NASA TR 202349, May 1997.